Energy transfer in nanowire solar cells with photon-harvesting shells

C. H. Peters,[a] A. R. Guichard, A. C. Hryciw, M. L. Brongersma, and M. D. McGehee
Department of Materials Science and Engineering, Stanford University, Stanford, California 94305, USA

(Received 17 March 2009; accepted 14 May 2009; published online 23 June 2009)

The concept of a nanowire solar cell with photon-harvesting shells is presented. In this architecture, organic molecules which absorb strongly in the near infrared where silicon absorbs weakly are coupled to silicon nanowires (SiNWs). This enables an array of 7-μm-long nanowires with a diameter of 50 nm to absorb over 85% of the photons above the bandgap of silicon. The organic molecules are bonded to the surface of the SiNWs forming a thin shell. They absorb the low-energy photons and subsequently transfer the energy to the SiNWs via Förster resonant energy transfer, creating free electrons and holes within the SiNWs. The carriers are then separated at a radial *p-n* junction in a nanowire and extracted at the respective electrodes. The shortness of the nanowires is expected to lower the dark current due to the decrease in *p-n* junction surface area, which scales linearly with wire length. The theoretical power conversion efficiency is 15%. To demonstrate this concept, we measure a 60% increase in photocurrent from a planar silicon-on-insulator diode when a 5 nm layer of poly[2-methoxy-5-(2′-ethyl-hexyloxy)-1,4-phenylene vinylene is applied to the surface of the silicon. This increase is in excellent agreement with theoretical predictions. © *2009 American Institute of Physics*. [DOI: 10.1063/1.3153281]

Electricity generated by silicon solar cells, which currently make up over 90% of the photovoltaic (PV) market, is still more expensive than that from conventional fossil fuels.[1] The most efficient silicon solar cells are made using single crystals, since grain boundaries promote recombination and impede charge transport. Much of the cost of manufacturing is associated with making single-crystal wafers. One exciting alternative approach is to grow crystalline nanowires from substrates using the vapor-liquid-solid method.[2,3] Another promising approach is to perform top-down etching of thin polycrystalline films to create arrays of nanowires that can be doped to form radial *p-n* junctions. Studies have shown advantages in carrier collection and device efficiency using radial *p-n* junction nanowires over planar devices of the same lower-quality material because the shorter distance minority carriers must travel to reach the *p-n* junction.[4,5] Additionally, because arrays of silicon nanowires (SiNWs) have a reduced effective index of refraction relative to bulk silicon, the reflectance compared to planar structures is significantly lower.[6] Using the optimal geometry of a tapered nanowire to achieve a graded index of refraction, the reflectance has been shown to approach zero across a broad range of wavelengths within the visible spectrum for angles of incidence up to 60°. This is in stark contrast to planar devices, which need to employ antireflection coatings and suffer large reflectance losses with increasing angles of incidence.[7] Recently, single SiNWs with radial *p-i-n* junctions were reported to have power conversion efficiencies (PCEs) of ~3.4%;[8] however, to date, groups that have produced arrays of vertically oriented radial SiNW solar cells have achieved low PCE (0.1%–0.50%).[3,9–12] A major contributor to the low efficiency is the high dark current, which scales linearly with the length of the wire. One approach to minimize this loss is to use shorter nanowires, but this requires a strategy for boosting absorption.

Here we model nanowire solar cells with photon-harvesting shells (PHSs) that utilize highly absorbing organic molecules coupled with SiNWs, 7 μm in length, to harness a significant portion of the solar spectrum above the bandgap of silicon. This dramatic reduction in nanowire length can reduce the large dark current that typically plagues SiNW solar cells. Using shorter nanowires has the added advantages of lower growth time and likely higher yield, leading to a more promising path to large-scale manufacturing. Modeling based on optical properties of the molecules, energy-transfer efficiency, and SiNW dimensions leads to an achievable PCE reaching as high as 15%.

A nanowire solar cell with PHSs that utilizes Förster resonant energy transfer (FRET) (Ref. 13) is shown schematically in Fig. 1. The PHS is made by adsorbing molecules to the passivating oxide layer on the surface of an array of SiNWs or, alternatively, directly to the silicon surface. The molecules absorb the incoming photons and subsequently transfer the excitons to the SiNWs via FRET. The *p-n* junc-

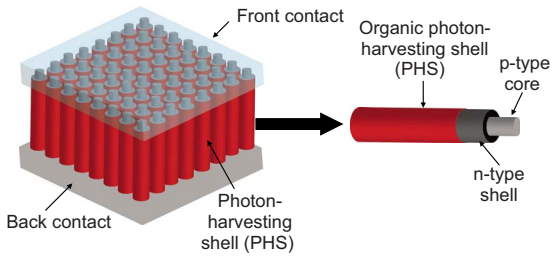

FIG. 1. (Color online) Schematic of a nanowire solar cell with a PHS. Organic molecules are chemically attached to the surface of the nanowires. The organic shell absorbs light and transfers the energy to the SiNWs via resonant energy transfer. The SiNWs have radial *p-n* junctions which selectively separate and transport the charges to the respective electrodes (shown in the isolated nanowire to the right).

[a]Electronic mail: chp3742@stanford.edu.

 © 2009 American Institute of Physics

Downloaded 30 Jun 2009 to 171.67.216.23. Redistribution subject to AIP license or copyright; see http://jap.aip.org/jap/copyright.jsp

tion in the SiNWs then selectively directs the electrons and holes to the appropriate electrodes, as is the case in a typical silicon solar cell. The molecules do not participate in charge transport and are only responsible for light absorption and energy transfer. Hence, these cells are very different from the family of cells known as dye-sensitized solar cells.[14,15]

Resonant energy transfer has been used in organic PVs to both broaden the absorption spectrum[16] and enhance exciton harvesting over larger distances.[17] This process occurs when an exciton residing on an excited chromophore (donor) undergoes a nonradiative transfer to a separate chromophore in its ground state (acceptor). The rate of transfer between the two chromophores is proportional to $1/r^6$,[13] where r is the separation distance. The rate of transfer from the donor to a two-dimensional sheet of acceptor molecules goes as $1/x^4$ (Ref. 18) and to a three-dimensional semi-infinite slab as $1/x^3$,[18,19] where x is the perpendicular distance of the donor from the surface of the acceptor. This distance dependence has been used to describe energy transfer to metal films,[18,20,21] between dyes in layered Langmuir–Blodgett structures,[22–24] in heterostructure OLEDs,[25] and from polymers to amorphous silicon structures.[26] In our system, where the radius of curvature of the nanowire is very large relative to the organic molecule, we can approximate the molecule as sitting on a semi-infinite slab of silicon and thus utilize the $1/x^3$ transfer rate distance dependence. The transfer rate in this case is given by

$$k_f(x) = \frac{C_A}{\tau}\frac{\pi}{6}\frac{R_o^6}{x^3}, \tag{1}$$

$$R_o^6 = \frac{9000\ \ln(10)K^2Q_D}{128\pi^5 n^4 N_A}\int F_D(\lambda)\varepsilon_A(\lambda)\lambda^4 d\lambda, \tag{2}$$

where R_o is the Förster radius,[13] τ is the lifetime of the exciton, and C_A (Ref. 27) is the acceptor density. Equation (2) shows the dependence of the Förster radius on the photoluminescence quantum efficiency (PLQE) of the donor Q_D, the index of refraction of the material between the donor and acceptor n, the relative transition dipole-dipole orientation factor K^2, and on the overlap of the donor emission spectrum $F_D(\lambda)$ and acceptor molar absorptivity $\varepsilon_A(\lambda)$. The Förster radius R_o is the distance at which there is a 50% energy transfer efficiency (ETE) for a point-to-point system. In our geometry, with a semi-infinite array of acceptor atoms, we can further calculate the point-to-slab distance x_{slab} at which there is a 50% ETE.

From Eq. (2) we see that the PLQE of the donor as well as the overlap between the donor emission and acceptor absorption spectra are critically important. This latter factor should influence our choice of donor molecules to use with silicon as the acceptor. Silicon's absorption coefficient is small for low-energy photons due to its indirect bandgap, increasing with photon energy as direct-bandgap transitions become possible. With this in mind, organic dyes that strongly absorb in the near IR should be chosen, allowing the silicon and the dyes to absorb the higher- and lower-energy photons, respectively. The use of two dyes through coattachment in equal amounts on the nanowires would provide broader near-IR absorption since strongly absorbing dyes typically have narrow absorption spectra. Figure 2(a) shows the absorption and emission spectra of two hypothetical near-IR dyes, which display typical characteristics of absorption and photoluminescence (PL). With silicon as the acceptor, and assuming a PLQE of 70% for both dyes, we arrive at R_o and x_{slab} values of 1.6 and 7.7 nm for dye A and 1.5 and 5.7 nm for dye B. The fact that the two dyes have similar Förster radii is surprising given the large shift in emission spectra. The overlap integral in Eq. (2) suggests that R_o should decrease as we shift to longer wavelengths due to the decreasing molar absorptivity $\varepsilon_A(\lambda)$ of silicon. However, this is offset by the λ^4 factor, resulting from the optical density of states for the acceptor and donor. This overall behavior of R_o is critically important since absorbing photons in the near IR is essential for high-efficiency SiNW solar cells.

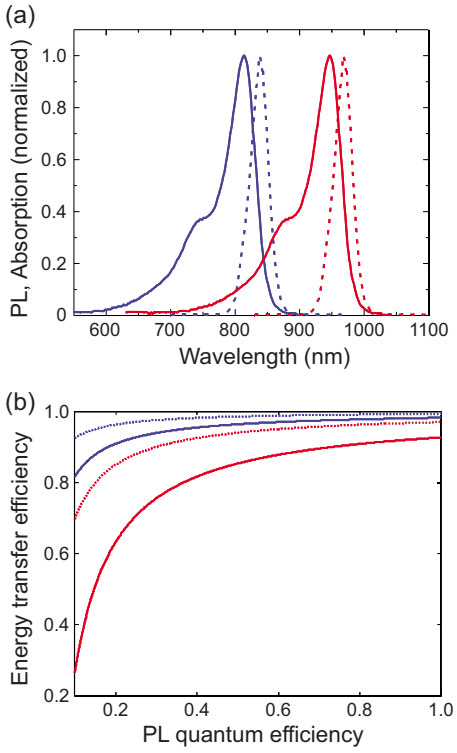

FIG. 2. (Color online) (a) Dye A absorption (blue) and PL (blue dashed) with dye B absorption (red) and PL (red dashed) for two hypothetical dyes. Dyes with molar extinction coefficients of greater than 2×10^5 M^{-1} cm^{-1} that absorb between 700 and 1000 nm are available commercially, although modifications for proper attachment to SiO_2 are required. (b) ETE as a function of dye PL efficiency for Dyes A (blue) and B (red). The solid and dashed lines are for x values of 2.7 nm and 1.7 nm, respectively. From the much weaker variation of the dashed curves compared to the solid curves, it is clear that it is important to carefully control the dye–silicon separation to achieve a high ETE for arbitrary dyes.

Attaching a dye to the native oxide layer creates a minimum distance between the center of the dye and the silicon surface of ~2.7 nm. Using the values for R_o and x_{slab} found above, energy transfer efficiencies of 96% and 90% can be achieved for dyes A and B, respectively. As earlier stated, the PLQE of the dye is important to consider. R_o scales as $(\text{PLQE})^{1/6}$, which dampens the negative impact of a lower PLQE, although clearly a dye with a value greater than 0.5 is desirable [Fig. 2(b)]. A more important parameter is x, the

Downloaded 30 Jun 2009 to 171.67.216.23. Redistribution subject to AIP license or copyright; see http://jap.aip.org/jap/copyright.jsp

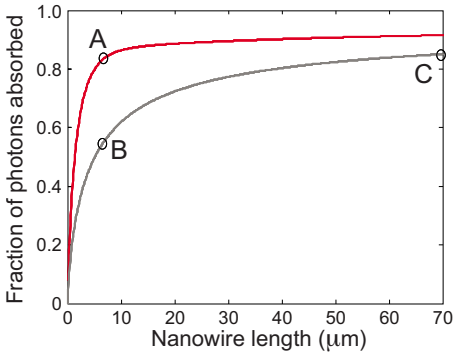

FIG. 3. (Color online) Fraction of photons above the bandgap of silicon that are absorbed with bare SiNWs (gray) and with dyes A and B attached to the nanowires (red) as a function of nanowire length. The nanowires are 50 nm in diameter with a center-to-center distance of 70 nm. Dyes A and B are assumed to have equal surface coverage with a molar absorptivity of 2×10^5 M^{-1} cm^{-1} and surface concentration on the wires of 7.5×10^{13} cm^{-2}.

distance between the center of the dye and the silicon surface. The dashed curves in Fig. 2(b) show the ETE for the two dyes when x decreases from 2.7 to 1.7 nm. Achieving such small separation distances is possible by functionalizing silicon dioxide and bare silicon surfaces.[28,29] When functionalizing the surface of silicon, it is important to passivate dangling bonds in order to minimize losses from surface recombination. High-quality thermally grown oxides as well as more novel techniques using methyl groups have been shown to be effective.[30–32]

Knowing the ETE, the absorption enhancement can be determined. Figure 3 shows the fraction of photons absorbed above the bandgap of silicon as a function of nanowire length. This model assumes nanowires of 50 nm diameter with a center-to-center distance of 70 nm. Absorption by the nanowires is calculated based on the bulk absorption coefficient of silicon as a function of wavelength together with the volume of silicon as a function of nanowire diameter, length, and spacing. Absorption by the PHS is calculated based on the surface area of the nanowires and assumed dye coverage of 7.5×10^{13} molecules/cm^2. We ignore reflection, scattering, and waveguide effects that tend to increase absorption, allowing an upper limit to be set on the length of the wires required to absorb a given fraction of photons. The diameter of the wires was chosen to maximize surface area for dye attachment while allowing for the depletion region to be fully contained within the wire, allowing the full realization of the built-in potential without the need for degenerate doping levels. Decreasing the diameter of the wires further would allow a higher density of wires, enabling the use of shorter wires to absorb the same amount of light but preventing the full realization of this built-in potential. We assume equal concentrations of dyes A and B on the nanowires. We see that 7 μm SiNWs alone absorb ~56% of the photons (Fig. 3, point "B") but with the attachment of the two dyes, ~84% of the photons are absorbed (point "A")—a boost in absorption of 50%. Plots of the optical density of the system as a function of wavelength (not shown) reveal that over half of the unabsorbed photons lie above 970 nm, the cutoff for the dye absorption. Taking into account this absorption and subsequent ETE to the silicon, while ignoring any reflection or recombination losses in the wires themselves, yields a short-circuit current density (J_{sc}) of ~36 mA/cm^2 for 7 μm SiNWs coated with the dyes. Achieving the same J_{sc} without using the dyes enabled by the PHS would require 70-μm-long SiNWs (point "C'). A factor of 10× reduction in nanowire length will impact the dark current and series resistance of the device. The voltage drop due to series resistance, however, is small for radial p-n junction nanowires. With doping levels of 10^{18} cm^{-3}, an electron mobility of 270 cm^2 V^{-1} s^{-1}, J_{sc}=36 mA cm^{-2}, and 70-μm-long nanowires, the voltage drop along the wire is on the order of 10^{-6} V. Lowering this by a factor of 10 provides a negligible improvement. However, since the dark current scales linearly with p-n junction surface area, reducing the wire length will lower the dark current, which is a much more important effect.

To understand the impact of a reduction in dark current on the device efficiency, we considered a theoretical study of radial junction nanowire solar cells performed by Atwater and co-workers.[4] In this work, it is shown that 100-μm-long SiNWs with a radius of 100 nm can achieve a J_{sc} of ~38 mA cm^{-2} and a V_{oc} of ~0.38–0.58 V, the exact value of which depends on the doping density in the wires as well as the trap density in the depletion and quasineutral regions. Nanowires with larger concentrations of traps in the depletion region $N_r > 3\times10^{15}$ cm^{-3} experience sharp declines in V_{oc} as the length of the nanowire increases. Using PHSs, we were able to achieve a similar J_{sc} of 36 mA cm^{-2} using 7-μm-long wires with 25 nm radii and 50% less packing density, which equates to a 7× reduction in p-n junction surface area. The relation

$$V_{oc} = \frac{k_B T}{q} \ln\left(\frac{J_{sc}}{J_o} + 1\right),$$

where k_B is the Boltzmann constant, T is the temperature (assumed to be 300 K), q is the charge, and J_o is the reverse saturation current, suggests that the open-circuit voltage should increase by ~10%–15%, the larger improvement being for higher defect density materials. A fill factor of 0.55 was reported for radial junction single nanowire solar cells,[8] although a value of 0.8 is theoretically achievable by keeping N_r below the value reported above. Taking the upper limit of open-circuit voltage (0.58 V) for wires of similar dimensions together with J_{sc} of 36 mA cm^{-2} and a fill factor of 0.65, we arrive at a PCE approaching 15% once we include the 10% increase in V_{oc} due to the shorter wires.

To demonstrate energy transfer between an organic molecule and silicon, we chose poly[2-methoxy-5-(2′-ethylhexyloxy)-1,4-phenylene vinylene (MEHPPV) as the donor. MEHPPV is an amorphous polymer that is soluble in many organic solvents, has a high absorption coefficient, good emission overlap with the absorption spectrum of silicon, and a PL efficiency of ~15% in neat films. Its solubility allows us to spin cast uniform thin films. We deposited a 5 nm layer of MEHPPV onto single-crystal silicon samples with varying oxide thicknesses [Fig. 4(a)].[33] Figure 4(b) shows the relative PL from each sample as a function of oxide thickness. For samples with thicker oxide spacer lay-

Downloaded 30 Jun 2009 to 171.67.216.23. Redistribution subject to AIP license or copyright; see http://jap.aip.org/jap/copyright.jsp

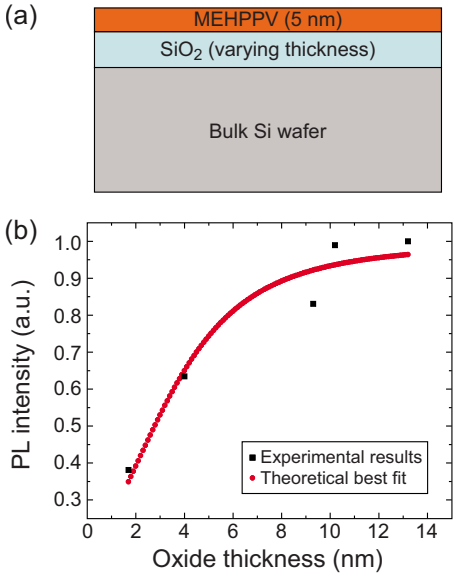

FIG. 4. (Color online) (a) Diagram of sample used to determine the Förster radius experimentally. The MEHPPV layer was kept constant at 5 nm while the oxide thickness was varied from ~1–10 nm. (b) Experimental PL data (black) and best fit (red) for MEHPPV on Si/SiO_2. Fitting yields R_o =1.3 nm and x_{slab}=4.9 nm are in good agreement with predicted values.

ers, the MEHPPV donor molecules sit further away from the silicon acceptor substrate, decreasing the ETE and thus increasing the measured PL intensity from the sample. Although the incident pump laser light can in general exhibit interference effects within the thin-film structure in such an experiment, resulting in variations in the MEHPPV excitation rate as the oxide thickness is changed, modeling has shown these effects to be negligible for the range of oxide thicknesses used here. Fitting the data to Eq. (1) yields R_o =1.3 nm and x_{slab}=4.9 nm. Using Eq. (2), we predict that R_o should be 1.3 nm and x_{slab} to be 5.0 nm in excellent agreement with our measurement. By solving the continuity equation for excitons within the MEHPPV layer, with the addition of the Förster energy transfer term, we find that the transfer efficiency of excitons to the silicon is 82%. The remaining 18% of the excitons naturally decay within the MEHPPV film.

The sensitization of silicon by organic molecules is known to result in an increase in photocurrent when illuminated at wavelengths where the molecules absorb.[34,35] To test some of the merits of our model, based on the absorption and subsequent ETE to silicon, we calculated and subsequently measured the increase in photocurrent from the device shown in Fig. 5 when MEHPPV was applied to the surface. We fabricated 80-nm-thick palladium contacts on lightly doped *n*-type silicon on insulator with a 50-nm-thick Si device layer using shadow-masked electron-beam evaporation. The samples were mounted in ceramic leadless chip carriers and wire bonded with aluminum wires. The chip carriers were then hermetically sealed, enabling device stability over the duration of the tests. The device layer thickness (50 nm) was on the order of the diameter of the wires we used in our previous optical models. The device was proved very stable in its electrical characteristics over a period of months, which provided excellent reproducibility. The cleaning process

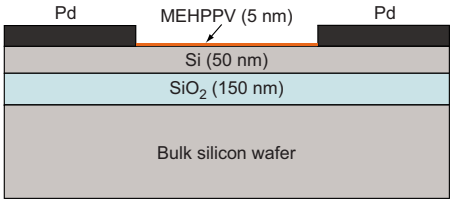

FIG. 5. (Color online) Device architecture used for measuring the external quantum efficiency spectrum of bare silicon and silicon with a 5 nm layer of MEHPPV. 80-nm-thick palladium (Pd) contacts were deposited on 50 nm of silicon, which was insulated from the bulk wafer by a 150 nm buried oxide layer. The spacing between contacts is 150 μm.

which employed acetone, isopropanol, and chlorobenzene had very little impact on the electrical characteristics. Finally, the planarity of the device allowed analytical modeling of the absorption rate throughout the structure, allowing us to predict the maximum enhancement we can expect in the photoresponse of the device.

Using transfer matrix methods[36] together with the tabulated optical constant data for silicon, SiO_2, and MEHPPV,[37,38] we modeled the electric field intensity and absorption rates throughout the device [Fig. 6(a)]. The devices without (dashed blue) and with (dashed red) a 5 nm layer of MEHPPV show the expected increase in absorption due to the MEHPPV. The dropoff in absorption at ~510 nm is due to interference effects from the 150-nm-thick buried oxide layer. Integration of the intensity of the field together with the absorption profiles of MEHPPV [Fig. 6(b)] and silicon leads to a theoretical absorption enhancement of 1.85×

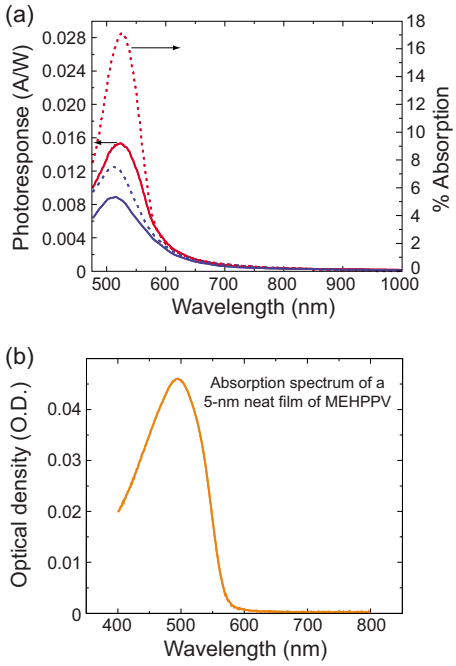

FIG. 6. (Color online) (a) Photoresponse of device under 1 V bias with (solid red) and without (solid blue) MEHPPV. The device with MEHPPV provides an ~1.6× increase in photocurrent. Shown also are the calculated percent absorptions for the device with (red dashed) and without (blue dashed) a 5 nm layer of MEHPPV. The absorption was modeled using the transfer-matrix method and tabulated optical constant data for the materials. The absorption profile due to interference effects explains the shape of the measured photoresponse spectrum. (b) The absorption spectrum of a 5-nm-thick layer of MEHPPV on quartz.

Downloaded 30 Jun 2009 to 171.67.216.23. Redistribution subject to AIP license or copyright; see http://jap.aip.org/jap/copyright.jsp

over a device without MEHPPV. Incorporating the ETE of 82% presented earlier yields a theoretical maximum enhancement of 1.7× in the overall photoresponse of the device.

The photoresponse of the device was experimentally determined by using a chopped 20 μm diameter beam from a Fianium supercontinuum fiber laser. The device was held at a 1 V bias and the current was measured as a function of wavelength using a lock-in amplifier[39] normalized with respect to incident power at each wavelength. Figure 6(a) shows the photoresponse of the device without (solid blue) and with (solid red) a 5 nm layer of MEHPPV. There is a clear enhancement in the photoresponse where MEHPPV absorbs light. The dropoff in photoresponse for both curves below ~510 nm follows the predicted profile of the absorption rate, calculated using transfer-matrix formalism. Comparison of the areas under the two photoresponse curves points to an overall enhancement of 1.6×, which is in good agreement with the maximum predicted value of 1.7×. Many diodes were tested with nearly identical results. As previously stated, we should expect surface recombination losses occurring at defect sites along the Si/SiO_2 interface, since the energy transfer process occurs near this interface. This will lower the predicted enhancement, as we have experimentally confirmed. To overcome this, proper surface passivation is important to ensure that the minority carrier diffusion length is sufficiently large, such that minority carriers can reach the *p-n* junction. Finally, closer inspection of the photoresponse curve and the absorption spectrum of MEHPPV reveal a slight redshift in the tail region of enhancement relative to the absorption of MEHPPV. We attribute this shift to the solid-state solvatochromic effect,[40] where stabilization of the excited state relative to the ground state can occur in the presence of a high dielectric material such as silicon. This can redshift both the absorption and emission spectra of MEHPPV, although we would not expect this effect to be uniform throughout the MEHPPV film since the molecules closest to the silicon would be affected most strongly.

In summary, 7-μm-long SiNW solar cells with a PHS enable the absorption of 85% of the photons above the bandgap of silicon. Without the PHS, 10× longer wires would be required to absorb the same amount of light. The shorter wires aid in lowering dark current, leading to a higher open-circuit voltage and PCE. We have developed a model for light absorption and energy transfer that matches well to the experimental results. This model predicts that with two separate organic dyes with appropriate absorption and emission spectra attached to 7-μm-long SiNWs, we should be able to achieve PCEs approaching 15%. This efficiency, combined with the ability to use lower quality material, offers a promising path to lower-cost solar energy. In addition, we expect the shorter wires to enable more reproducible and reliable fabrication methods, which are critical for commercialization. The major challenges for implementing this design are the growth of low trap density nanowires, well-passivated surfaces to reduce recombination effects, and methods for large-scale production. All of these challenges are currently being explored by the research community with promising advances in each area.[8,30,31,41]

The authors acknowledge the King Abdullah University of Science and Technology (KAUST) Center for Advanced Molecular Photovoltaics and the Global Climate and Energy Project at Stanford University for funding this project.

[1] N. Lewis, Science **315**, 798 (2007).
[2] A. M. Morales and C. M. Lieber, Science **279**, 208 (1998).
[3] E. C. Garnett and P. Yang, J. Am. Chem. Soc. **130**, 9224 (2008).
[4] B. M. Kayes, H. A. Atwater, and N. S. Lewis, J. Appl. Phys. **97**, 114302 (2005).
[5] Y. Zhang, L. Wang, and A. Mascarenhas, Nano Lett. **7**, 1264 (2007).
[6] L. Hu and G. Chen, Nano Lett. **7**, 3249 (2007).
[7] J. Zhu, Z. Yu, G. F. Burkhard, C. M. Hsu, S. T. Connor, Y. Xu, Q. Wang, M. D. McGehee, S. Fan, and Y. Cui, Nano Lett. **9**, 279 (2009).
[8] B. Z. Tian, X. L. Zheng, T. J. Kempa, Y. Fang, N. F. Yu, G. Yu, J. Huang, and C. M. Lieber, Nature (London) **449**, 885 (2007).
[9] T. H. Stelzner, M. Pietsch, G. Andra, F. Falk, E. Ose, and S. Christiansen, Nanotechnology **19**, 295203 (2008).
[10] L. Tsakalakos, J. Balch, J. Fronheiser, B. A. Korevaar, O. Sulima, and J. Rand, Appl. Phys. Lett. **91**, 233117 (2007).
[11] A. P. Goodey, S. M. Eichfeld, K. Lew, J. M. Redwing, and T. E. Mallouk, J. Am. Chem. Soc. **129**, 12344 (2007).
[12] J. R. Maiolo, B. M. Kayes, M. A. Filler, M. C. Putnam, M. D. Kelzenberg, H. A. Atwater, and N. S. Lewis, J. Am. Chem. Soc. **129**, 12346 (2007).
[13] T. Forster, Discuss. Faraday Soc. **27**, 7 (1959).
[14] B. O'Regan and M. Gratzel, Nature (London) **353**, 737 (1991).
[15] M. Law, L. E. Greene, A. Radenovic, T. Kuykendall, J. Liphardt, and P. Yang, J. Phys. Chem. B **110**, 22652 (2006).
[16] L. C. Chen, L. S. Roman, D. M. Johansson, M. Svensson, M. R. Andersson, R. A. J. Janssen, and O. Inganas, Adv. Mater. (Weinheim, Ger.) **12**, 1110 (2000).
[17] S. R. Scully, P. B. Armstrong, C. Edder, J. M. J. Frechet, and M. D. McGehee, Adv. Mater. (Weinheim, Ger.) **19**, 2961 (2007).
[18] H. Kuhn, J. Chem. Phys. **53**, 101 (1970).
[19] S. R. Scully and M. D. McGehee, J. Appl. Phys. **100**, 034907 (2006).
[20] D. E. Markov and P. W. M. Blom, Appl. Phys. Lett. **87**, 233511 (2005).
[21] D. E. Markov and P. W. M. Blom, Phys. Rev. B **72**, 161401 (2005).
[22] J. Hill, S. Y. Heriot, O. Worsfold, T. H. Richardson, A. M. Fox, and D. D. C. Bradley, Phys. Rev. B **69**, 041303 (2004).
[23] T. Del Cano, M. L. Rodriguez-Mendez, R. Aroca, and J. A. De Saja, Mater. Sci. Eng., C **22**, 161 (2002).
[24] K. Ray, H. Nakahara, A. Sakamoto, and M. Tasumi, Chem. Phys. Lett. **342**, 58 (2001).
[25] P. O. Anikeeva, C. F. Madigan, S. A. Coe-Sullivan, J. S. Steckel, M. G. Bawendi, and V. Bulovic, Chem. Phys. Lett. **424**, 120 (2006).
[26] V. Gowrishankar, S. R. Scully, A. T. Chan, M. D. McGehee, Q. Wang, and H. M. Branz, J. Appl. Phys. **103**, 064511 (2008).
[27] C_A is the acceptor density which is also used in the calculation of R_o, since R_o depends on the density of the acceptor, which in the case of silicon is 5.22×10^{22} cm^{-3}.
[28] A. Ulman, J. Am. Chem. Soc. **96**, 1533 (1996).
[29] J. M. Buriak, J. Am. Chem. Soc. **102**, 1271 (2002).
[30] H. Haick, P. T. Hurley, A. L. Hochbaum, P. Yang, and N. S. Lewis, J. Am. Chem. Soc. **128**, 8990 (2006).
[31] J. E. Green, S. J. Wong, and J. R. Heath, J. Phys. Chem. C **112**, 5185 (2008).
[32] B. Hoex, J. Schmidt, R. Bock, P. P. Altermatt, M. C. M. van de Sanden, and W. M. M. Kessels, Appl. Phys. Lett. **91**, 112107 (2007).
[33] The oxide thickness was measured using variable angle spectroscopic ellipsometry with a white light source. The MEHPPV thin film was spun cast from a chlorobenzene solution at 2000 rpm for 45 s in a nitrogen environment to prevent photo-oxidation. We excited the samples using a Spectra-Physics argon ion laser at 514 nm in a nitrogen environment to avoid photo-oxidation. PL from the samples was measured using a SpectraPro 500i triple grating monochromator and a semiconductor-cooled charge coupled device (CCD 128HB, Acton Research).
[34] C. Kelting, U. Weiler, T. Mayer, W. Jaegermann, S. Makarov, D. Wohrle, O. Abdallah, M. Kunst, and D. Schlettwein, Org. Electron. **7**, 363 (2006).
[35] T. Mayer, U. Weiler, E. Mankel, W. Jaegermann, C. Kelting, D. Schlettwein, N. Baziakina, and D. Wohrle, Renewable Energy **33**, 262 (2007).

Downloaded 30 Jun 2009 to 171.67.216.23. Redistribution subject to AIP license or copyright; see http://jap.aip.org/jap/copyright.jsp

[36]L. A. A. Pettersson, L. S. Roman, and O. Inganas, J. Appl. Phys. **86**, 487 (1999).
[37]*Handbook of Optical Constants of Solids*, edited by E. D. Palik (Academic, New York, 1976).
[38]M. Tammer and A. P. Monkman, Adv. Mater. (Weinheim, Ger.) **14**, 210 (2002).
[39]Care was taken to ensure that the measurements were made in the same location on the diode. Monochromatic excitation with wavelength from 400 nm to 1 μm was provided by a Fianium supercontinuum fiber laser sent through a monochromator. The excitation was chopped and fed into a preamplifier and read out on a lock-in amplifier (Stanford Research Systems SR810 DSP). The beam was focused through a Mitutoyo 50× objective to a spot size of 20 μm in diameter although the capabilities exist to reduce the diameter to the submicron level. The excitation power at 510 nm, the absorption peak of MEHPPV, was set at 100 mW/cm^2, the equivalent of one sun. The excitation spectrum was measured by a silicon photodiode prior to each measurement to ensure accurate normalization for each photocurrent action spectrum taken.
[40]C. Reichardt, *Solvents and Solvent Effects in Organic Chemistry*, 2nd ed. (VCH Publishers, New York, 1988).
[41]K. E. Plass, M. A. Filler, J. M. Spurgeon, B. M. Kayes, S. Maldonado, B. S. Brunschwig, H. A. Atwater, and N. S. Lewis, Adv. Mater. (Weinheim, Ger.) **21**, 325 (2009).

Downloaded 30 Jun 2009 to 171.67.216.23. Redistribution subject to AIP license or copyright; see http://jap.aip.org/jap/copyright.jsp